Stochastic Piecewise Linear Function Fitting with Application to Ultrasound Shear Wave Imaging*

Atul Ingle[1,2] Tomy Varghese[2,1], William Sethares[1], James Bucklew[1]

***Abstract*— Piecewise linear function fitting is ubiquitous in many signal processing applications. Inspired by an application to shear wave velocity imaging in ultrasound elastography, this paper presents a discrete state-space Markov model for noisy piecewise linear data and also proposes a tractable algorithm for maximum a posteriori estimation of the slope of each segment in the piecewise linear function. The number and locations of breaks is handled indirectly by the stochastics of the Markov model. In the ultrasound shear wave imaging application, these slope values have concrete physical interpretation as being the reciprocal of the shear wave velocities in the imaged medium. Data acquired on an ellipsoidal inclusion phantom shows that this algorithm can provide good contrast of around 6 dB and contrast to noise ratio of 25 dB between the stiff inclusion and surrounding soft background. The phantom validation study also shows that this algorithm can be used to preserve sharp boundary details, which would otherwise be blurred out if a sliding window least squares filter is applied.**

I. INTRODUCTION

Hepatocellular carcinoma is a leading cause of cancer related deaths in both developed and developing countries throughout the world [1]. Radiofrequency or microwave ablation is a common treatment of smaller tumors especially in patients that are not candidates for liver surgery or a transplant. Monitoring the ablation process is paramount to ensure that the right volume of liver tissue is treated because untreated cancer cells may cause the tumor to recur.

Ultrasound shear wave velocity (SWV) imaging is gaining popularity as a promising tool for differentiating regions of the imaged tissue based on stiffness. In particular, this imaging mode can be of immense use for monitoring tumor ablation procedures where clinicians must accurately control the size of the ablation to ensure that almost all the cancerous cells in the tissue are treated. At a high level, SWV images are produced by tracking a shear wave pulse in the imaging plane. Tracking is achieved using the popular "time of arrival" method [2] which records the time at which the shear wave pulse arrives at different locations away from the source. The slope of this time of arrival plot is therefore equal to the reciprocal of the wave speed, also known as "slowness" [3].

This paper presents a model for noisy piecewise linear data which is applied to the SWV estimation problem. Test data is acquired on a tissue mimicking phantom using an electrode vibration setup, called electrode vibration elastography (EVE) [6]. This technique is minimally invasive in the sense that it requires only the use of small (on the order of a 100 microns) displacements to be applied to the ablation needle.

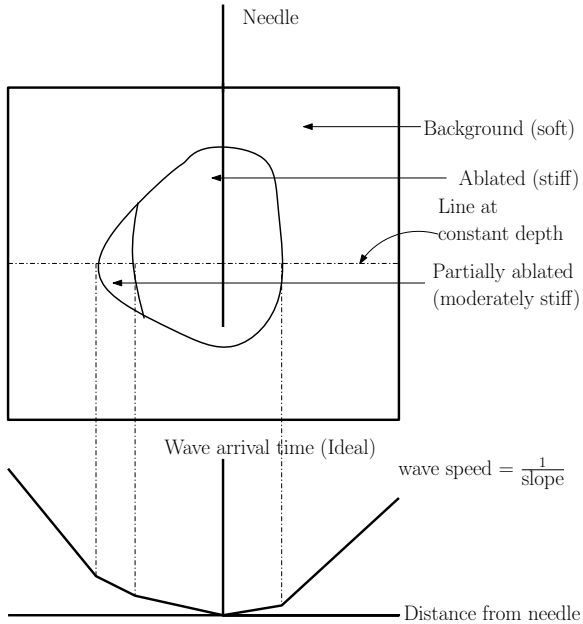

Fig. 1. Cross-sectional view of the phantom is shown with the inclusion, partially ablated region and surrounding background material. The needle is used to generate a shear wave pulse which is tracked at different locations away from the needle over lines of constant depth. This gives a wave arrival time plot. The shear wave velocity is equal to the reciprocal of the slope of this plot.

II. THEORY

A theoretical model for piecewise linear data is presented in this section. A computational algorithm for estimating slopes from noisy data using this model is also discussed. A physical interpretation of the model will become apparent in Section III which describes the shear wave imaging experiment. It is also worth noting that the slope estimation algorithm presented here is general enough to handle piecewise linear data arising in many other applications as well.

A. Model for Piecewise Linear Data

It is assumed that the user has a reliable estimate of the minimum and maximum possible slope values that can be present in the underlying noiseless data. For instance, in the

*This work was supported in part by NIH-NCI grants R01CA112192-S103 and R01CA112192-05. Atul Ingle is the corresponding author. Email: ingle@wisc.edu.

[1]Department Electrical and Computer Engineering,

[2]Department of Medical Physics, University of Wisconsin-Madison, Madison WI 53706 USA.

978-1-4244-7929-0/14/$26.00 ©2014 IEEE

shear wave imaging application there are physical limits on the wave speed in tissues. Hence, without loss of generality, it can be assumed that the slopes lie in the unit interval $[0, 1]$. This interval is discretized to M levels so that the "states" for the slope values is the finite set $\mathcal{S} = \{0, \frac{1}{M-1}, \ldots, \frac{M-2}{M-1}, 1\}$. A total of N equidistant data samples are available at discrete sampling locations $1 \leq n \leq N$. A Markov structure is imposed on the sequence S_n of slope values as follows. Let S_0 have a uniform probability mass function on the set $\mathcal{S}$. For $n \geq 1$, let $S_n = S_{n-1}$ with probability p, otherwise S_n is chosen uniformly randomly from $\mathcal{S} \setminus \{S_{n-1}\}$. The piecewise linear function is realized by accumulating these slopes, i.e. $X_0 = 0$ with probability 1, and $X_{n+1} = X_n + S_{n+1}$ for $n \geq 1$. Finally, the observed function values follow the relation $Y_n = X_n + W_n$ where W_n are i.i.d. normally distributed with zero mean and (unknown) variance σ^2.

The posterior density function of the unknown function values given the data can be easily derived by exploiting the Markov structure:

$$\begin{aligned} p(x_1, \ldots, x_N | y_1, \ldots, y_N) &\propto p(y_1, \ldots, y_N | x_1, \ldots, x_N) \\ &= p(y_1|x_1)p(x_1|x_0) \\ &\quad \prod_{i=2}^{N} p(y_i|x_i)p(x_i|x_{i-1}, x_{i-2}). \end{aligned}$$

Taking the logarithm, and using the relation $x_i = \sum_{j=1}^{i} s_j$ (for $i \geq 1$), the maximum a posteriori (MAP) estimation problem for the slope values s_n can be written as

$$\begin{aligned} (s_1^{\mathsf{MAP}}, \ldots, s_N^{\mathsf{MAP}}) &= \underset{(s_1,\ldots,s_N)\in\mathcal{S}^N}{\arg\max} -\frac{1}{2\sigma^2}\sum_{i=1}^{N}(y_i - \sum_{j=1}^{i} s_j)^2 \\ &\quad + \sum_{i=2}^{N} \log\left(p\,\delta_{s_n = s_{n-1}} + \frac{1-p}{M-1}\delta_{s_n \neq s_{n-1}} \right) \quad (1) \end{aligned}$$

where δ is the Kronecker delta function which evaluates to 1 when the condition in the subscript is true and 0 otherwise.

Note that this model is parametrized by two unknown parameters p and σ^2 which will affect the final result. Intuitively, if p is very close to 1, one expects to see longer runs of constant slope values, i.e. a fit with few change points. Moreover, a larger value of σ^2 can potentially outweigh the second term in the maximization problem (1) resulting in a (trivial) least squares line fit. In practice, the value of p can be selected based on the number of slope change points one expects to see in the raw data. The value of σ^2 can be estimated from the raw data by calculating its sample variance after detrending.

B. Slope Estimation Algorithm

The MAP estimation problem can be solved using a Viterbi-like algorithm by traversing a trellis of possible slope values at each index $1 \leq n \leq N$ [7]. However, the trellis search can become computationally burdensome for large N because of the $\sum_{i=1}^{j} s_i$ term in the objective function which depends on all the slope values into the past. An approximate optimization is used in this paper in the interest of processing speed. The objective function to be maximized is non-differentiable (due to the presence of Kronecker delta functions). Moreover, the discrete nature of the problem makes it challenging to use standard optimization routines which rely on a "hill climbing" scheme in a continuous space. Therefore, it is more convenient to work with a continuous version of the problem by approximating the Kronecker delta function using a narrow Gaussian spike $\delta_{s_n = s_{n-1}} \approx e^{-(s_n - s_{n-1})^2/k^2}$ where k is used to control the width of the spike. Moreover, the slope values are now allowed to vary freely in the interval $[0, 1]$. This leads to the following relaxed formulation:

$$\begin{aligned} \underset{(s_1,\ldots,s_N)\in[0,1]^N}{\arg\max} \Bigg[& -\frac{1}{2\sigma^2}\sum_{i=1}^{N}(y_i - \sum_{j=1}^{i} s_j)^2 \\ & + \sum_{i=2}^{N} \log\Big(p\, e^{-(s_n - s_{n-1})^2/k^2} + \\ & \frac{1-p}{M-1}(1 - e^{-(s_n - s_{n-1})^2/k^2}) \Big) \Bigg]. \quad (2) \end{aligned}$$

This optimization is solved using a sequential quadratic programming (SQP) routine, in which each constituent quadratic program is solvable in polynomial time [5]. The result is then quantized to the set $\mathcal{S}$. Although there is no theoretical guarantee that this is in fact close to the exact MAP estimate obtained by solving the original problem in (1), the results in Section IV on real data indicate that it works well in practice.

III. MATERIALS AND METHODS

A. Tissue Mimicking Phantom

The tissue mimicking phantom used for data acquisition consists of a gel block with oil droplets in a gelatin matrix. The stiffness can be controlled by varing the proportion of oil in the matrix; details on the construction of this phantom can be found in the paper by Madsen *et al.* [4]. The phantom contains an ellipsoidal inclusion of higher shear modulus than the surrounding background material. A stainless steel needle is firmly glued to the center of the inclusion and mimics the ablation needle in an actual tumor ablation procedure. A smaller region of intermediate stiffness is present on one side of the inclusion to mimic a partially ablated area. A cross-section of the phantom is shown in the top panel in Fig. 1.

B. Shear Wave Generation and Imaging

A shear wave pulse is generated by vibrating the needle vertically using an actuator (Physik Instrumente, Germany) and radiofrequency ultrasound echo data is acquired simultaneously (Ultrasonix SonixTouch, Canada) using triggered acquisition. A pulse actuation of 100 μm amplitude and 20 ms width is used. Pseudo-high frame rate echo data is acquired using a phase locked acquisition technique [6] which relies on multiple vibrations of the needle to acquire vertical bands of data and assembling these to form complete frames of echo data. A linear array transducer with center

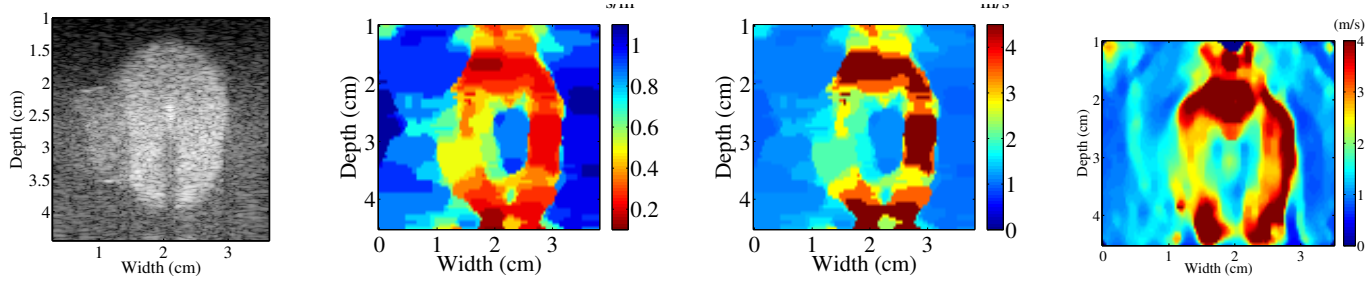

(a) B-mode (b) Slowness (s/m) (c) Velocity (m/s) (d) Velocity LSQ (m/s)

Fig. 2. Results from shear wave velocity reconstruction using approximate stochastic piecewise linear fitting. (a) B-mode image of the phantom, (b) slowness map and (c) shear wave velocity image obtained by calculating the reciprocal of the slowness image. For comparison, a SWV image (d) obtained from a windowed least squares slope estimation algorithm is also shown.

TABLE I

SHEAR WAVE VELOCITY ESTIMATES

	Inclusion	Par. Abl.	Background
SWV (m/s)	2.73 ± 0.68	1.91 ± 0.53	1.26 ± 0.15
SNR (dB)	15.5 ± 3	12.8 ± 3.6	21.8 ± 3.8
SWV LSQ (m/s)	3.03 ± 0.98	2.11 ± 0.32	1.33 ± 0.32
SWV SSI (m/s)	2.8 ± 1.1	2.3 ± 0.8	1.3 ± 0.4

Estimated mean shear wave velocity and SNR for the three different regions in the experimental phantom obtained are shown. For comparison, the shear wave velocities obtained using a 7-point moving average least squares filter (LSQ), and phantom measurements using a commercial shear wave imaging system (SSI) are also shown.

TABLE II

IMAGE QUALITY

	Incl./Par.Abl.	Par.Abl./Backgr.	Incl./Backgr.
CNR (dB)	7.46 ± 6.5	12.1 ± 6.7	25.1 ± 4.7
C (dB)	3.07 ± 1.6	3.67 ± 0.73	6.74 ± 1.8
CNR LSQ (dB)	4.98 ± 2.9	16.1 ± 2.9	15.9 ± 2.6
C LSQ (dB)	3.16 ± 0.6	4.07 ± 0.6	7.23 ± 0.7

Contrast (C), and contrast-to-noise ratios (CNR) (in dB) obtained from shear wave velocity estimates for three pairs of regions are shown. Standard deviations shown here are calculated using ten independent datasets, after converting to dB. Corresponding values obtained from a 7-point moving average least squares filtering method are also shown.

frequency set at 5 MHz was used. Ten independent datasets were acquired for image quality evaluation.

Measurements were also made with a commercial Supersonic Imagine system (Aix-en-Provence, France) using the clinical shear wave velocity imaging mode (SSI).

C. Data Processing

A one-dimensional crosscorrelation based displacement estimation algorithm is used to determine the displacement at each pixel in the image over time (axial 2 mm windows, 75% overlap). The peak of the displacement profile at each pixel is used to estimate the arrival time of the shear wave front at different locations away from the needle [2]. This produces a wave arrival time plot over lines of constant depth as shown in the lower panel of Fig. 1.

The optimization problem in (2) is then solved to fit piecewise linear functions both to the left and right sides of the needle along lines of constant depth. $k = 10^{-3}$ is used to approximate the Kronecker delta function with a narrow Gaussian pulse. The value of $p = 0.95$ is used (expecting around 5 slope changes per 100 data samples) and $\sigma^2 = 1$ is used as an estimate for the noise variance. Estimated local slope values are then displayed as a slowness map. The reciprocal of these slope values are used to generate SWV images[1]. Three different regions of interest (ROI) of size 1 cm $\times$ 2 cm are selected in each image and three different image quality statistics are calculated. The signal to noise ratio (SNR) is defined as $SNR = 20\log_{10}(\mu/\lambda)$, contrast as $C = 20\log_{10}(\mu_1/\mu_2)$ and contrast to noise ratio as $CNR = 20\log_{10}((\mu_1 - \mu_2)^2/(\lambda_1^2 + \lambda_2^2))$ [8], where μ denotes the mean; λ^2 is the sample variance calculated over any ROI; and subscripts denote two different ROIs. For comparison, a sliding window linear least squares method is also used to estimate shear wave velocities. A 7 point moving window is used, and the slope is estimated by fitting a line using 3 neighboring data points on either side of each data point. The image quality metrics described above are recalculated with this method.

IV. RESULTS

A B-mode image of the phantom together with the slowness image and SWV image are shown in Fig. 2. Note that the three different stiffness areas are easily visible in the B-mode image of the phantom because the materials were designed with different acoustic echogenicities on purpose. Delineation in actual tissues is not easily noticeable in B-mode. High stiffness regions can be clearly visualized with well demarcated boundaries in both the slowness and SWV images. The low velocity artifact near the center of the inclusion is due to lack of tracking quality in regions very close to the needle. The reconstruction quality obtained using the algorithm presented in this paper provides sharper

[1]The final goal of shear wave elastography is to image shear moduli; SWV is only used as a surrogate for stiffness. Alternatively, to avoid calculating the reciprocal of noisy data, the slowness image can also be used as the surrogate.

boundary details compared to the standard least squares filtering method (Fig. 2(c) vs. (d)).

The estimated SWV using ROIs in 10 different datasets are shown in Table I. These agree quite well with the standard least squares method and also with the measurements made using SSI. Image quality metrics are shown in Table II. The highest contrast to noise ratio of 25 dB and contrast of over 6 dB is obtained between the stiff inclusion and soft background material. The partially ablated and background regions are the most difficult to discern, even visually in Fig. 2 and is also indicated by the lower CNR and C values. The contrast values obtained from the least squares filtering method is almost equal to that from the algorithm proposed in this paper. The CNR values are much lower with least squares filtering.

V. DISCUSSION AND CONCLUSIONS

This paper presented a stochastic model for piecewise linear functions and applied this model to estimate slopes in arrival time plots encountered in electrode vibration based shear wave elastography. The algorithm is approximate in that it only solves a relaxed version of the full MAP estimation problem. However, results using phantom experiments suggest that it provides useful visualization of stiff inclusion boundaries. Quantization of the slope values into M user defined bins provides a useful speed vs. accuracy tradeoff. This method can be implemented on any commercial ultrasound scanner capable of producing high frame rate radiofrequency ultrasound echo data frames.

Note that there are a variety of artifacts present in the SWV images that are specific to EVE. The time of arrival estimator is reliable only when the shear wave front travels purely in a lateral direction away from an ideal line source (the needle in this case). This assumption breaks down in areas above and below the inclusion, which may be the cause for high velocity artifacts in these regions. Moreover, the low velocity artifact near the center of the inclusion has been consistently observed in previous EVE studies as well. They should not pose a serious obstacle in applications because it is more crucial to locate the outer boundary as the tissue immediately surrounding the needle is surely completely ablated.

REFERENCES

[1] G Lee, AI Schafer. Cecil medicine: expert consult premium 24th ed. Elsevier Health Sciences, 2011, ch. 202.

[2] ML Palmeri, MH Wang, JJ Dahl, KD Frinkley, KR Nightingale, "Quantifying Hepatic Shear Modulus in vivo Using Acoustic Radiation Force," *Ultrasound Med. Biol.*, vol. 34, no. 4, 2008, pp. 546–558.

[3] S. Stein, M. Wysession, Basic Seismological Theory, in: An Introduction to Seismology, Earthquakes, and Earth Structure, 1st ed., Malden, MA: Blackwell, 2003, Ch. 2, Sec. 2.5.7, pp. 69.

[4] EL Madsen, MA Hobson, H Shi, T Varghese, GR Frank, "Tissue-mimicking Agar/gelatin Materials for Use in Heterogeneous Elastography Phantoms," *Phys Med Biol.*, vol. 50, 2005, pp. 5597–5618.

[5] J. Nocedal and S. Wright, *Numerical Optimization*, 2nd ed., New York: Springer, 2006.

[6] RJ DeWall, T Varghese, EL Madsen, "Shear wave velocity imaging using transient electrode perturbation: phantom and ex vivo validation," *Medical Imaging, IEEE Transactions on* vol. 30, no. 3, 2011, pp. 666-678.

[7] LR Rabiner "A tutorial on hidden Markov models and selected applications in speech recognition," Proceedings of the IEEE vol. 77 no. 2, February 1989, pp. 257–286.

[8] T. Varghese, J. Ophir, An analysis of elastographic contrast to noise ratio, Ultrasound in Medicine and Biology, vol. 24, no. 6, July 1998, pp. 915–924.